Electromagnetic scattering by densely packed particulate ice at radar wavelengths: exact theoretical results and remote-sensing implications

Michael I. Mishchenko[1,*] and Li Liu[1,2]

[1]NASA Goddard Institute for Space Studies, 2880 Broadway, New York, New York 10025, USA

[2]Columbia University and NASA Goddard Institute for Space Studies, 2880 Broadway, New York, New York 10025, USA

*Corresponding author: mmishchenko@giss.nasa.gov

Received 12 February 2009; accepted 23 March 2009;
posted 1 April 2009 (Doc. ID 107388); published 22 April 2009

We use the numerically exact superposition T-matrix method to compute electromagnetic scattering characteristics of a macroscopic volume of a discrete random medium filled with wavelength-sized spherical particles with a refractive index typical of water ice at centimeter wavelengths. Our analysis demonstrates relative strengths of various optical observables in terms of their potential remote-sensing content. In particular, it illustrates the importance of accounting for the forward-scattering interference effect in the interpretation of occultation measurements of planetary rings. We show that among the most robust indicators of the amount of multiple scattering inside a particulate medium are the cross-polarized scattered intensity, the same-helicity scattered intensity, and the circular polarization ratio. We also demonstrate that many predictions of the low-packing-density theories of radiative transfer and coherent backscattering are applicable, both qualitatively and semi-quantitatively, to densely packed media. © 2009

OCIS codes: 030.1670, 030.5620, 290.4210, 290.5850.

1. Introduction

Scattering of electromagnetic waves by densely packed particulate media is a subject of utmost importance to the discipline of remote sensing of the Earth and other solar system objects. In particular, the knowledge of scattering properties of densely packed particulate ice is needed for the interpretation of radar observations of terrestrial ice sheets [1], the Moon [2], Mercury [3], Galilean satellites of Jupiter [4], and Saturn's rings [5]. Similarly, definitive interpretation of bidirectional remote-sensing observations of snow, soil, desert, and regolith surfaces at visible wavelengths [6–10] requires an accurate scattering theory directly based on the Maxwell equations.

On the one hand, reliable and efficient numerically exact techniques for the computation of single-scattering properties of arbitrarily shaped individual objects (particles) with sizes smaller than or on the order of the wavelength have been available for almost three decades and have been applied quite extensively [11,12]. Furthermore, the radiative transfer theory (RTT) has become a direct corollary of classical electromagnetics [13] and allows one to compute electromagnetic scattering by large objects consisting of randomly and sparsely distributed particles, such as clouds. On the other hand, the rigorous analytical theory of electromagnetic scattering by densely packed particulate media (e.g., particulate surfaces of planets) is still in progress [14] and is

0003-6935/09/132421-06$15.00/0
© 2009

often substituted by empirical or semi-empirical approaches with vaguely defined or unknown accuracy and applicability range.

However, recent theoretical advances and the continuously improving efficiency of scientific workstations have led to the emergence of a new branch of statistical electromagnetics in which the problem of scattering by macroscopic media composed of densely packed, randomly positioned particles is addressed using direct, numerically exact computer solutions of the Maxwell equations [15–18]. Although this approach cannot be used yet to directly model electromagnetic scattering by morphologically complex particulate planetary surfaces, it can already be applied to macroscopic media consisting of hundreds of randomly positioned particles. This allows one to do the following:

- Obtain useful and instructive numerically exact results.
- Use theory as an ideal "controlled laboratory experiment" in which all microphysical properties of the random particulate medium are known and controlled precisely, can be varied one by one, and can be unambiguously linked to accompanying changes in the scattering properties of the medium.
- Derive unequivocal conclusions regarding the qualitative and quantitative effects of multiple scattering (including coherent backscattering (CB), otherwise known as weak localization of electromagnetic waves), particle microphysics, and packing density on actual observable quantities.
- Test the applicability of asymptotic low-packing-density theories of radiative transfer and coherent backscattering [13] to densely packed particulate media.
- Derive meaningful remote-sensing implications.

It is especially important to recognize in this regard that optical phenomena such as CB are theoretical concepts [19,20], and their relevance to actual remote sensing observations cannot be established by simply comparing one set of experimental results to another and thereby avoiding accurate theoretical modeling.

Given the ubiquitous presence of particulate water ice throughout the solar system, in this paper we apply the above rigorous approach to study electromagnetic scattering by a simple model of a densely packed macroscopic volume filled with wavelength-sized ice particles. We assume a refractive index value typical of ice at centimeter radar wavelengths. Our model cannot be expected to replicate exactly the diverse morphologies of particulate ice media formed in varying natural conditions and has practical limitations on the number of constituent particles. However, it is sufficiently versatile and representative to permit a robust and instructive analysis of electromagnetic scattering by densely packed particulate media, especially in combination with recent results obtained for substantially different particle refractive indices [16].

2. Model and Numerical Results

Our model of a macroscopic volume of discrete random medium is a spherical volume filled with N identical nonoverlapping spherical particles [Fig. 1(a)]. The size parameters of the volume and the particles are fixed at $k_1R = 50$ and $k_1r = 4$, respectively, where k_1 is the wave number in the empty space surrounding the particles, R is the volume radius, and r is the particle radius. The number of particles is varied from 20 to 391, which corresponds to filling factors (or packing densities) ρ ranging from 1% to 20%. The particle refractive index is fixed at $m = 1.787 + i0.003$ and corresponds to (weakly contaminated) water ice at centimeter wavelengths [21].

To model random particle positions within the spherical volume, we follow the approach outlined in [16]. Specifically, we use one randomly configured N-particle group [22] and average relevant optical observables over all possible orientations of this configuration with respect to the laboratory coordinate system. This approach yields, in effect, an infinite continuous set of random realizations of the scattering volume and allows us to take full advantage of the highly efficient orientation averaging technique afforded by the numerically exact superposition T-matrix method [23].

We assume that the statistically random particulate volume is illuminated by a plane electromagnetic wave or a parallel quasi-monochromatic beam of light propagating in the direction of the unit vector $\hat{\mathbf{n}}^{\mathrm{inc}}$ [Fig. 1(b)]. The observation direction is specified by the unit vector $\hat{\mathbf{n}}^{\mathrm{sca}}$. Since the scattering properties of the particulate volume are averaged over all orientations of the N-particle group, we can simplify the discussion by using the scattering plane for defining the Stokes parameters of the incident (inc) and scattered (sca) light. The transformation of the Stokes parameters in the far-field zone of the volume is then written in terms of the normalized Stokes scattering matrix [13,24,25]:

$$\begin{bmatrix} I^{\mathrm{sca}} \\ Q^{\mathrm{sca}} \\ U^{\mathrm{sca}} \\ V^{\mathrm{sca}} \end{bmatrix} \propto \begin{bmatrix} a_1(\Theta) & b_1(\Theta) & 0 & 0 \\ b_1(\Theta) & a_2(\Theta) & 0 & 0 \\ 0 & 0 & a_3(\Theta) & b_2(\Theta) \\ 0 & 0 & -b_2(\Theta) & a_4(\Theta) \end{bmatrix} \begin{bmatrix} I^{\mathrm{inc}} \\ Q^{\mathrm{inc}} \\ U^{\mathrm{inc}} \\ V^{\mathrm{inc}} \end{bmatrix}, \tag{1}$$

where Θ is the scattering angle [Fig. 1(b)]. The phase function $a_1(\Theta)$ is normalized according to

$$\frac{1}{2}\int_0^{\pi} \mathrm{d}\Theta \, \sin\Theta a_1(\Theta) = 1. \tag{2}$$

The most relevant and instructive numerical results are summarized in Figs. 1(c)–1(l). For reference, we also show the results computed for a single isolated spherical particle. The phase function $a_1(\Theta)$

characterizes the angular distribution of the scattered intensity provided that the incident radiation is unpolarized, while the ratio $-b_1(\Theta)/a_1(\Theta)$ gives the corresponding degree of linear polarization. If the incident radiation is polarized linearly in the scattering plane (i.e., $Q^{\mathrm{inc}} = I^{\mathrm{inc}}$ and $U^{\mathrm{inc}} = V^{\mathrm{inc}} = 0$), then the angular distributions of the copolarized and cross-polarized scattered intensities are given by $\frac{1}{2}(I^{\mathrm{sca}} + Q^{\mathrm{sca}}) \propto \frac{1}{2}[a_1(\Theta) + 2b_1(\Theta) + a_2(\Theta)]$ and $\frac{1}{2}(I^{\mathrm{sca}} - Q^{\mathrm{sca}}) \propto \frac{1}{2}[a_1(\Theta) - a_2(\Theta)]$, respectively. Finally, if the incident radiation is polarized circularly in the counterclockwise direction when looking in the direction of propagation (i.e., $Q^{\mathrm{inc}} = U^{\mathrm{inc}} = 0$ and $V^{\mathrm{inc}} = I^{\mathrm{inc}}$), then the angular distributions of the same-helicity and opposite-helicity scattered intensities are given by $\frac{1}{2}(I^{\mathrm{sca}} + V^{\mathrm{sca}}) \propto \frac{1}{2}[a_1(\Theta) + a_4(\Theta)]$ and $\frac{1}{2}(I^{\mathrm{sca}} - V^{\mathrm{sca}}) \propto \frac{1}{2}[a_1(\Theta) - a_4(\Theta)]$, respectively. The linear, μ_{L}, and circular, μ_{C}, polarization ratios are defined as the ratio of the cross-polarized to copolarized scattered intensities and the ratio of the same-helicity to the opposite-helicity scattered intensities, respectively [4]. Their angular profiles are given by

$$\mu_{\mathrm{L}} = \frac{I^{\mathrm{sca}} - Q^{\mathrm{sca}}}{I^{\mathrm{sca}} + Q^{\mathrm{sca}}} = \frac{a_1(\Theta) - a_2(\Theta)}{a_1(\Theta) + 2b_1(\Theta) + a_2(\Theta)}, \tag{3}$$

$$\mu_{\mathrm{C}} = \frac{I^{\mathrm{sca}} + V^{\mathrm{sca}}}{I^{\mathrm{sca}} - V^{\mathrm{sca}}} = \frac{a_1(\Theta) + a_4(\Theta)}{a_1(\Theta) - a_4(\Theta)}. \tag{4}$$

The computations took 140 days on a Linux server with 8 GB of RAM and 2.50 GHz CPU speed. By far the most time-consuming computation was that for the scattering volume with $N = 391$ (116 days).

3. Discussion

In full agreement with the results of [16] obtained for refractive indices 1.32 and 1.5, Fig. 1(d) demonstrates two fundamental consequences of increasing the number of particles in the scattering volume. First, the constructive interference of light singly scattered by the component particles in the exact forward direction causes a strong and narrow forward-scattering enhancement. This feature is further detailed in Fig. 1(c), which reveals that the forward-interference effect saturates for filling factors exceeding 0.1, i.e., when the geometrical projection of the volume on the plane normal to $\hat{\mathbf{n}}^{\mathrm{inc}}$ becomes almost completely filled with particles. Accordingly, the light blue curve essentially represents the diffraction pattern for a solid scatterer with radius R.

The results shown in Fig. 1(c) confirm our conclusion [16,26] that the forward-interference effect is a general far-field property of multiparticle groups [27]. Although it is unimportant in monostatic radar observations, it must be taken into account in analyses of occultation measurements of planetary rings. For example, it has been suggested that the distribution of particles across Saturn's rings is not uniform at the scale of tens and hundreds of meters (e.g., see [28] and references therein). If so, the angular profile of the transmitted signal must be a complex convolution of a narrow ρ-dependent forward-scattering feature indicative of the inhomogeneity scale and a broader feature indicative of the size of the ring particles. It is obvious that ignoring the forward-interference effect in the process of inversion of occultation results is likely to cause a significant overestimation of the particle size.

The second effect of increasing N on the phase functions is to make them progressively smooth and featureless at side-scattering angles. This trait is quite consistent with the numerical predictions based on the RTT [13,29] despite the latter being an asymptotic low-packing-density limit of statistical electromagnetics [13,26]. This result demonstrates that although multiple scattering is a purely mathematical idealization rather than a real physical phenomenon [26], it remains a useful interpretation tool even in the case of densely packed particles not positioned in the far-field zones of each other. Indeed, we could think of the smoothing effect of increasing N on the angular distribution of the scattered intensity as being a consequence of increasing the amount of "multiple scattering" whereby light undergoing many "scattering events" caused by the individual particles "forgets" the initial incidence direction $\hat{\mathbf{n}}^{\mathrm{inc}}$ and is more likely to contribute equally to all exit directions $\hat{\mathbf{n}}^{\mathrm{sca}}$.

Similarly, the most obvious effect of increasing the number of particles in the volume on $-b_1(\Theta)/a_1(\Theta)$ is to smooth out oscillations in the polarization curves and, on average, make this ratio closer to zero [Fig. 1(e)]. This trait could also be interpreted in the RTT terms by noticing that the main contribution to Q^{sca} comes from the first order of scattering, whereas light scattered many times still contributes substantially to the outgoing intensity I^{sca}. The only exception is the range of scattering angles strongly influenced by the forward-interference effect. Here the high-frequency oscillations in the phase function cause antiphased oscillations in the ratio $-b_1(\Theta)/a_1(\Theta)$.

Another expected consequence of increasing N in the limit of low packing density is a growing phase function peak centered at exactly the backscattering direction and caused by the CB effect [19]. This backscattering peak is quite visible indeed in the phase functions computed for the particle refractive indices 1.32 and 1.5 [16], which suggests the applicability of the inherently low-packing-density concept of CB even to particulate media with filling factors as large as 24%. Therefore, it comes as somewhat of a surprise that a similar CB peak appears to be absent in the phase functions computed for $m = 1.787 + i0.003$ [Fig. 1(f)]. However, a close examination of the curves for $\rho = 0.1$ and 0.2 in Fig. 1(f) reveals a subtle feature with an angular width of a few degrees, consistent with the interference origin of CB.

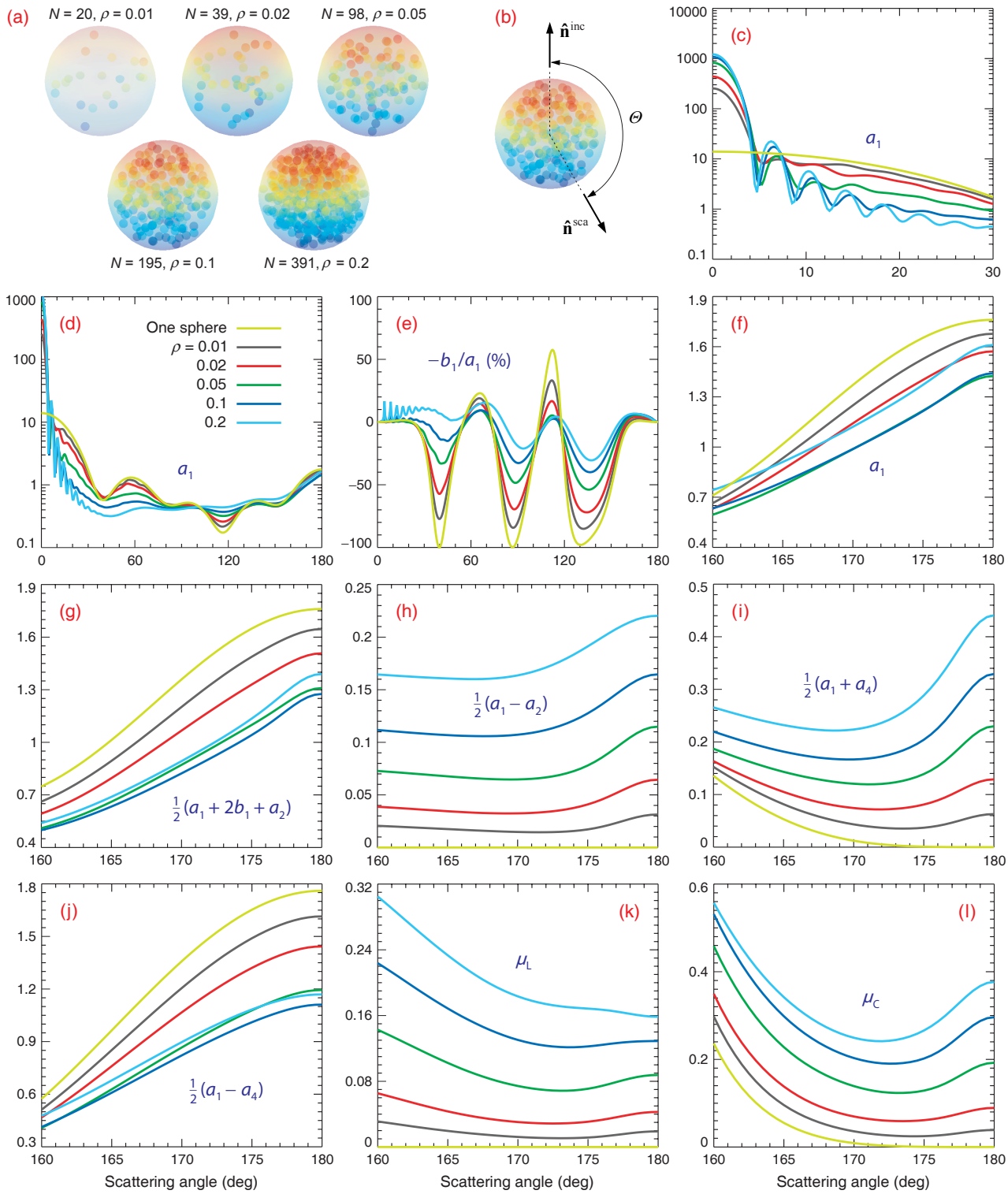

Fig. 1. (a) Macroscopic spherical scattering volume filled with N randomly positioned spherical ice particles. (b) Scattering geometry. (c)–(l) Scattering characteristics of the macroscopic volume as functions of the particle filling factor and scattering angle.

This result obviously indicates that a pronounced backscattering peak in the single-particle phase function [see the light green curve in Fig. 1(f)] can almost completely mask the CB peak.

There is no doubt that the CB peak should become more clearly identifiable for a much larger and optically thicker scattering volume. Indeed, then the angular width of the CB peak can be expected to decrease and its amplitude can be expected to increase. Still, the absence of a noticeable CB peak is often attributed to a negligible amount of multiple scattering in a strongly absorbing particulate

medium. Our results obtained for weakly absorbing particles obviously suggest that this attribution is not generally correct.

The same fully applies to the copolarized scattered intensity $\frac{1}{2}[a_1(\Theta) + 2b_1(\Theta) + a_2(\Theta)]$. Indeed, this optical observable exhibits strong CB peaks for particles with the refractive indices 1.32 and 1.5 [16] but only a hint of a peak for particles with $m = 1.787 + i0.003$ [see the curves for $\rho = 0.1$ and 0.2 in Fig. 1(g)]. In the case of the opposite-helicity scattered intensity $\frac{1}{2}[a_1(\Theta) - a_4(\Theta)]$, only particles with $m = 1.32$ cause a pronounced CB peak [16].

Comparison of Figs. 1(h), 1(i), and 1(l) with the corresponding results in [16] reveals that the cross-polarized scattered intensity $\frac{1}{2}[a_1(\Theta) - a_2(\Theta)]$, the same-helicity scattered intensity $\frac{1}{2}[a_1(\Theta) + a_4(\Theta)]$, and the circular polarization ratio μ_C are among the most robust detectors of the effect of CB. Specifically, CB always causes a pronounced backscattering peak with an angular width unequivocally indicative of its interference origin. This is an important conclusion since the presence of a CB peak can usually be attributed to a significant amount of multiple scattering in a weakly absorbing particulate medium. This makes the angular profiles of $\frac{1}{2}[a_1(\Theta) - a_2(\Theta)]$, $\frac{1}{2}[a_1(\Theta) + a_4(\Theta)]$, and μ_C valuable remote-sensing observables.

On the other hand, CB can cause either a backscattering enhancement or a backscattering "depression" in the linear polarization ratio μ_L, depending on particle microphysical properties as well as on the optical thickness of the particulate medium [cf. Fig. 1(k) and the corresponding results in [16]]. The low-packing-density computations for spherical and spheroidal particles shown on Plates 14.6.5 and 14.6.6 and Fig. 14.6.6 of [13] suggest that in the case of a semi-infinite particulate slab the effect of CB is always to reduce μ_L. However, Fig. 14.6.4 in [13] shows that CB can cause a backscattering depression for optically thin slabs that gradually evolves into a backscattering enhancement for optically thicker slabs. The exact dense-medium results in Fig. 1(k) appear to corroborate this low-packing-density prediction and demonstrate how a backscattering enhancement at $\Theta > 175°$ transforms into a backscattering depression with N growing from 20 to 391. This result implies that the backscattering angular profile of μ_L may not be a reliable and unequivocal detector of the effect of CB.

Large backscattering values of the linear and circular polarization ratios are usually considered sensitive indicators of the amount of multiple scattering inside the particulate medium (cf. Figs. 1(k) and 1(l)). Although this is correct in many cases, one should not forget the potentially strong effect of particle nonsphericity, which can cause large μ_L and μ_C values even for light scattered just once [13,24,30].

4. Conclusions

In summary, our analysis of numerically exact scattering results for densely and sparsely packed particulate media demonstrates the relative strengths and weaknesses of various remote-sensing observables in terms of their potential information content. It emphasizes the critical importance of accounting for the forward-scattering interference effect in analyses of occultation measurements of planetary rings. It also suggests that among the most robust detectors of CB and thus indicators of the amount of multiple scattering inside a particulate medium are the cross-polarized scattered intensity, the same-helicity scattered intensity, and the circular polarization ratio. Finally, it demonstrates that many predictions of the low-packing-density theories of radiative transfer and CB are applicable, both qualitatively and semi-quantitatively, to densely packed media.

One can, of course, think of various extensions of this work such as analyses of the potential effects of nonsphericity [31] and polydispersity of the constituent particles. Obviously, such analyses as well as computations for larger scattering volumes with significantly greater numbers of constituent particles will require much more powerful computers than the one we used for this study.

We are grateful to Joop Hovenier, Daniel Mackowski, Victor Tishkovets, Gorden Videen, and two anonymous reviewers for valuable comments and suggestions. This research was funded by the NASA Radiation Sciences Program managed by Hal Maring.

References

1. E. Rignot, "Backscatter model for the unusual radar properties of the Greenland Ice Sheet," J. Geophys. Res. **100**, 9389–9400 (1995).
2. S. Nozette, P. Spudis, M. Robinson, D. Bussey, C. Lichtenberg, and R. Bonner, "Integration of lunar polar remote-sensing data sets: evidence for ice at the lunar south pole," J. Geophys. Res. **106**, 23253–23266 (2001).
3. J. K. Harmon, M. A. Slade, R. A. Vélez, A. Crespo, M. J. Dryer, and J. M. Johnson, "Radar mapping of Mercury's polar anomalies," Nature **369**, 213–215 (1994).
4. S. J. Ostro, "Planetary radar astronomy," Rev. Mod. Phys. **65**, 1235–1279 (1993).
5. P. D. Nicholson, R. G. French, D. B. Campbell, J.-L. Margot, M. C. Nolan, G. J. Black, and H. J. Salo, "Radar imaging of Saturn's rings," Icarus **177**, 32–62 (2005).
6. V. Rosenbush, N. Kiselev, V. Avramchuk, and M. Mishchenko, "Photometric and polarimetric opposition phenomena exhibited by solar system bodies," in *Optics of Cosmic Dust*, G. Videen and M. Kocifaj, eds. (Kluwer Academic, 2002), pp. 191–224.
7. G. Videen, Ya. Yatskiv, and M. Mishchenko, eds., *Photopolarimetry in Remote Sensing* (Kluwer Academic, 2004).
8. M. I. Mishchenko, V. K. Rosenbush, and N. N. Kiselev, "Weak localization of electromagnetic waves and opposition phenomena exhibited by high-albedo atmosphereless solar system objects," Appl. Opt. **45**, 4459–4463 (2006).
9. Yu. Shkuratov, S. Bondarenko, V. Kaydash, G. Videen, O. Muñoz, and H. Volten, "Photometry and polarimetry of particulate surfaces and aerosol particles over a wide range of phase angles," J. Quant. Spectrosc. Radiat. Transfer **106**, 487–508 (2007).
10. H. Zhang and K. J. Voss, "Bidirectional reflectance measurements of closely packed natural and prepared particulate

surfaces," in *Light Scattering Reviews 3*, Springer Praxis Books (Springer, 2008), pp. 279–327.
11. M. I. Mishchenko, J. W. Hovenier, and L. D. Travis, eds., *Light Scattering by Nonspherical Particles: Theory, Measurements, and Applications* (Academic, 2000).
12. F. M. Kahnert, "Numerical methods in electromagnetic scattering theory," J. Quant. Spectrosc. Radiat. Transfer **79–80**, 775–824 (2003).
13. M. I. Mishchenko, L. D. Travis, and A. A. Lacis, *Multiple Scattering of Light by Particles: Radiative Transfer and Coherent Backscattering* (Cambridge University, 2006).
14. V. P. Tishkovets, "Incoherent and coherent backscattering of light by a layer of densely packed random medium," J. Quant. Spectrosc. Radiat. Transfer **108**, 454–463 (2007).
15. K. K. Tse, L. Tsang, C. H. Chan, K. H. Ding, and K. W. Leung, "Multiple scattering of waves by dense random distributions of sticky particles for applications in microwave scattering by terrestrial snow," Radio Sci. **42**, RS5001 (2007).
16. M. I. Mishchenko, L. Liu, D. W. Mackowski, B. Cairns, and G. Videen, "Multiple scattering by random particulate media: exact 3D results," Opt. Express **15**, 2822–2836 (2007).
17. S. Tseng, "Optical characteristics of a cluster of closely-packed dielectric spheres," Opt. Commun. **281**, 1986–1990 (2008).
18. Y. Okada and A. A. Kokhanovsky, "Light scattering and absorption by densely packed groups of spherical particles," J. Quant. Spectrosc. Radiat. Transfer (to be published).
19. Yu. N. Barabanenkov, Yu. A. Kravtsov, V. D. Ozrin, and A. I. Saichev, "Enhanced backscattering in optics," Prog. Opt. **29**, 65–197 (1991).
20. V. L. Kuz'min and V. P. Romanov, "Coherent phenomena in light scattering from disordered systems," Phys.-Usp. **39**, 231–260 (1996).
21. C. Mätzler, ed., *Thermal Microwave Radiation: Applications for Remote Sensing* (IET Press, 2006).
22. D. W. Mackowski, "A simplified model to predict the effects of aggregation on the absorption properties of soot particles," J. Quant. Spectrosc. Radiat. Transfer **100**, 237–249 (2006).
23. D. W. Mackowski and M. I. Mishchenko, "Calculation of the T matrix and the scattering matrix for ensembles of spheres," J. Opt. Soc. Am. A **13**, 2266–2278 (1996).
24. M. I. Mishchenko, L. D. Travis, and A. A. Lacis, *Scattering, Absorption, and Emission of Light by Small Particles* (Cambridge University, 2002), http://www.giss.nasa.gov/~crmim/books.html.
25. J. W. Hovenier, C. van der Mee, and H. Domke, *Transfer of Polarized Light in Planetary Atmospheres—Basic Concepts and Practical Methods* (Springer, 2004).
26. M. I. Mishchenko, "Multiple scattering, radiative transfer, and weak localization in discrete random media: unified microphysical approach," Rev. Geophys. **46**, RG2003 (2008).
27. A. P. Ivanov, A. Ya. Khairullina, and T. N. Kharkova, "Experimental detection of cooperative effects in a scattering volume," Opt. Spectrosc. **28**, 204–207 (1970).
28. C. C. Porco, J. W. Weiss, D. C. Richardson, L. Dones, T. Quinn, and H. Throop, "Simulations of the dynamical and light-scattering behavior of Saturn's rings and the derivation of ring particle and disk properties," Astron. J. **136**, 2172–2200 (2008).
29. J. E. Hansen and L. D. Travis, "Light scattering in planetary atmospheres," Space Sci. Rev. **16**, 527–610 (1974).
30. J. M. Dlugach and M. I. Mishchenko, "Diffuse and coherent backscattering of polarized light: polarization ratios for a discrete random medium composed of nonspherical particles," J. Quant. Spectrosc. Radiat. Transfer **106**, 21–32 (2007).
31. E. Zubko, Yu. Shkuratov, M. Hart, J. Eversole, and G. Videen, "Backscattering of agglomerate particles," J. Quant. Spectrosc. Radiat. Transfer **88**, 163–171 (2004).